coatings

MDPI

Article

Optical Behavior of Curcuminoid Hybrid Systems as Coatings Deposited on Polyester Fibers

Florentina Monica Raduly, Valentin Rădiţoiu *, Alina Rădiţoiu, Violeta Purcar, Georgiana Ispas, Adriana Nicoleta Frone, Raluca Augusta Gabor and Cristian-Andi Nicolae

Laboratory of Functional Dyes and Related Materials, National Research and Development Institute for Chemistry and Petrochemistry—ICECHIM, 060021 Bucharest, Romania; monica.raduly@icechim.ro (F.M.R.); coloranti@icechim.ro (A.R.); violeta.purcar@icechim.ro (V.P.); georgiana.ispas23@yahoo.com (G.I.); ciucu_adriana@yahoo.com (A.N.F.); ralucagabor@yahoo.com (R.A.G.); ca_nicolae@yahoo.com (C.-A.N.)
* Correspondence: vraditoiu@icechim.ro

Abstract: The recent development of the "eco-friendly" current has brought to the attention of researchers natural dyes that are biodegradable, do not cause allergies and generally have anti-UV protection, and antioxidant and antibacterial properties. In this study, we aimed to obtain hybrid materials of the dye–host matrix type, by using the sol–gel process. The silica network was generated by tetraethylorthosilicates and modified with organic siloxane derivatives: phenyltriethoxysilane, 3-glycidoxypropyltriethoxysilane, dimethoxydimethylsilane and dimethoxydiphenylsilane. The nanocomposites obtained by embedding curcumin in siloxane matrices were deposited on polyester fabric and evaluated for their properties, relative to the type of organic network modifier used. Fabrics covered with curcuminoid hybrid systems provide a hydrophobic surface, have fluorescent properties and a UPF +50, and, therefore, they can be used in various fields where it is necessary for textiles to provide signaling, self-cleaning or protection properties against ultraviolet radiation. The coated textile materials have very good resistance properties after several repeated washing cycles, and maintain the original UV protection factor at high values even after washing or during rubbing tests.

Keywords: curcumin; fluorescence; UV protection; hybrid coatings; sol–gel; polyester fibers

Citation: Raduly, F.M.; Rădiţoiu, V.; Rădiţoiu, A.; Purcar, V.; Ispas, G.; Frone, A.N.; Gabor, R.A.; Nicolae, C.-A. Optical Behavior of Curcuminoid Hybrid Systems as Coatings Deposited on Polyester Fibers. *Coatings* **2022**, *12*, 271. https://doi.org/10.3390/coatings12020271

Academic Editor: Günter Motz

Received: 23 December 2021
Accepted: 15 February 2022
Published: 17 February 2022

1. Introduction

Textile materials used in signaling applications for road equipment, sports equipment, materials for special services (firefighters, police, rescue) or advertising are colored with fluorescent dyes, which cause a deep increase in color [1–3]. Usually, for such equipment, a polyester support is used, and the dyeing is performed by mass coloration. This process is widespread and intensively used for all types of markings and signaling on textile support. The issues related to this process consist of a limited range of shades, short fluorescence lifetime, several paths of extinguishing fluorescence by interactions of dye molecules with the support and molecules of the same type and requirements of resistance to photodegradation which leads to the need for frequent replacement of signaling material [4–6]. In order to increase their quality, a series of research works has been carried out on the modification of textile surfaces with nanosols generated by sol–gel processes [7]. By applying these processes, textiles with repellent, flame retardant, electroconductive, antimicrobial or UV protection properties are frequently obtained [8–12]. One of the most important factors for the application of nanosols on textile fibers is the adhesion between the substrate and the coating material. To date, there are various studies on the use of silica matrix as a host for the immobilization of anionic dyes and the surface dyeing of polyester and viscose [13,14], as well as for coating some natural textile fibers with direct or nonionic dyes in sol–gel systems [11,15]. The recent development of the "eco-friendly" current has brought to the attention of researchers some of the special properties of natural dyes,

which are biodegradable, do not cause allergies and generally provide UV protection. They can function as antioxidants or have antibacterial activity, but, unfortunately, have poor light resistance [16–19]. Thus, in order to compensate for this shortcoming, the dyes are manufactured using transitional metal salts as mordants, and performing alkalis and other various predyeing treatments in the presence of steam, ozone or plasma, depending on the type of natural/synthetic fibers [20–23], for generating anchoring groups for dyes and/or metal ions on their surfaces.

Curcumin (1,7-bis (4-hydroxy-3-methoxy phenyl)-1,6-heptadiene-3,5-dione (1E-6E)) is the main compound separated from the mixture of dyes extracted from Turmeric root. The dye has been used in the treatment of various diseases [24–26] and for dyeing natural fibers in shades of yellow-brown, since antiquity [27]. In recent years, it has been the most widely used natural dye in studies for biomedical applications, as a food additive or for textile coatings [28]. Due to the antioxidant, antiviral and antimicrobial properties of curcumin, the dye has been conditioned in various forms, such as nanoemulsions, nanoparticles or nanocomposites to be deposited on textiles used for dressing and protective clothing with anti-UV or antimicrobial properties [29–32]. For the applications of the dye in textile support, different methods of dye deposition were tried using high pressure, supercritical CO_2, ultrasounds, sol–gel impregnation processes, or exhaustion methods. Each of these methods leads to the development of different types of dye conditioning to improve the dyeing properties and compatibility with new types of natural or synthetic fibers [33–35]. The diversity of the application fields of curcumin and its derivatives results from the complexity of the properties given by a molecular structure, which is seemingly simple. The keto-enol structure and isomerism of the acetylacetone skeleton (which depends decisively on the pH and polarity of the environment in which it is located or on the existing neighborhoods in an immobile structure, in which the freedom of movement of the molecule is limited) determines the tautomeric equilibrium and, consequently, the optical properties of the compounds. Thus, the ketone form leads to a hypsochromic effect by interrupting the conjugation to the methylene carbon atom (sp^3 hybridized), the molecule functioning as the sum of the two isolated chromophores. If these chromophores are different, two absorption bands characteristic of the two chromophores will appear in the visible spectrum separately, and if they are identical (i.e., the molecule is symmetrical) the absorption band will have a single maximum of double intensity, corresponding to the chromophore. The enol form leads to extensive conjugation and the formation of an intramolecular hydrogen bond. The absorption band of the extended chromophore will most likely have a wide shape that is frequently asymmetrical and batochromic, shifted from the previous ones. The most pronounced bathochromic shift would be obtained if the 4-substituted aromatic nuclei have different substituents and one of them were a strong electron donor (e.g., dialkyl amine) and the other a strong electron acceptor (e.g., nitro). In this way, the electronic contrast between the two ends of the extended chromophore would be maximum and, therefore, the most accentuated bathochromic displacement would be recorded. The influence of the substituents in the case of two substituted aromatic nuclei would have a less pronounced effect, because of the position situated closer to the heptadienone system but especially because of steric constrains that can lead to a limitation of the conjugation [36–39].

In this work we studied the conditioning of curcumin in the form of hybrid silica nanosols by the sol–gel process and the surfaces obtained after depositing film-forming materials on polyester fabrics. Curcumin was entrapped in the hybrid silica network modified with organosilane derivatives, following the compatibilization of the dye dopped silica matrices with the surface of polyester synthetic fibers. At the same time, the preservation of the optical properties of the dye after its incorporation in the siloxane host matrices was investigated.

2. Materials and Methods

2.1. Materials

To obtain nanosols, without further purification, the following substances were used: organic silane derivatives (Figure 1) from Aldrich, Saint Louis, MO, USA, with purity ≤95%, tetraethylortosilicate, TEOS (Figure 1a), phenyltriethoxysilane, PTES (Figure 1b), 3-glycidoxypropyltriethoxysilane, GPTES (Figure 1c), dimethoxydimethylsilane, DMDMS (Figure 1d), dimethoxydiphenylsilane, DMDPS (Figure 1e), hydrochloric acid (0.1 N, HCl, Chimreactiv, Bucharest, Romania) ethanol (96%, EtOH, Chimreactiv, Bucharest, Romania), N-methylimidazole (99%, NMI, Aldrich, Saint Louis, MO, USA) and tetrahydrofuran (99%, THF, Merck, Kenilworth, NJ, USA). The dye (Figure 1f) with a structure similar to that of natural curcumin, was synthesized in the laboratory in microwaves and purified, by using an already known method [40]. The fabric used was 100% polyester, PES (Figure 1g), (specific weight of 95 g/m^2, tensile strength, (kg) warp 81 and weft 63, tearing strength, (kg) warp 2724 and weft 2621) obtained from Matasea Romana, Romania. The polyester fabric used for the experiments is of plane wave type, having a yarn linear density of 36 tex and warp/weft density of 28/26 threads/cm.

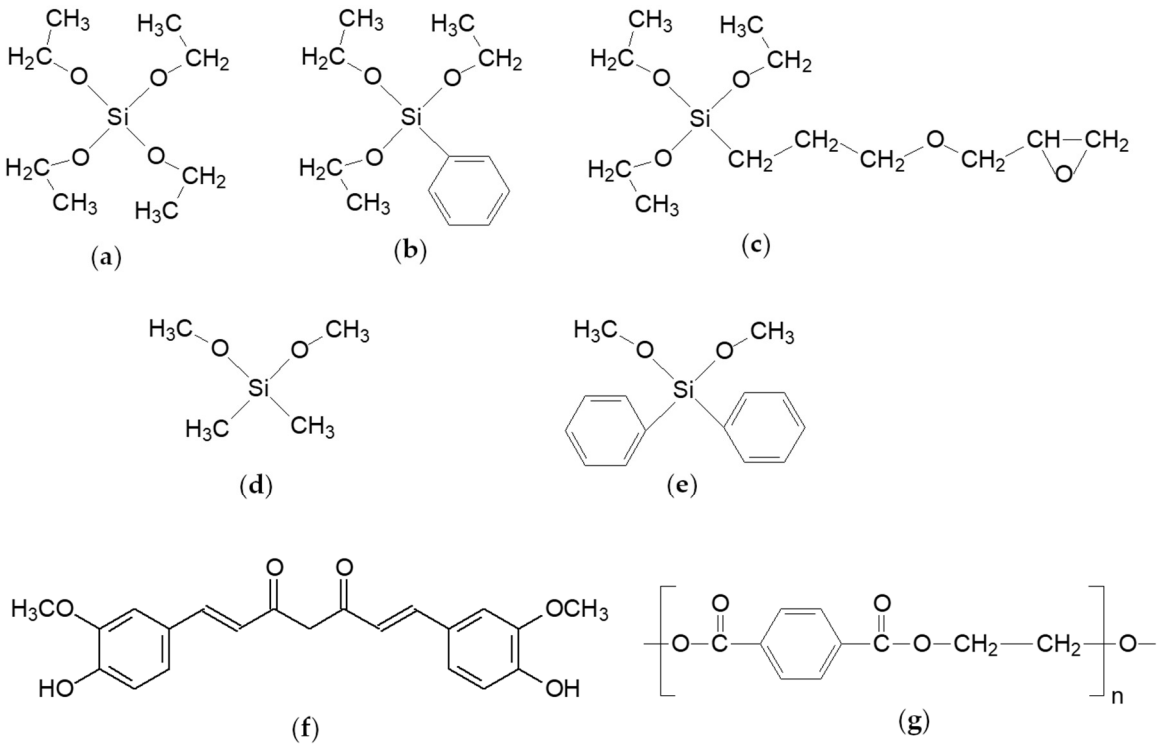

Figure 1. Raw materials used to obtain coated textile fibers: (**a**)—tetraethoxylortosilicate, (**b**)—phenyltriethoxysilane, (**c**)—3-glycidoxypropyltriethoxysilane, (**d**)—dimethoxydimethylsilane, (**e**)—dimethoxydiphenylsilane, (**f**)—curcumin, (**g**)—polyester fabric.

2.2. The Method of Obtaining Nanosols, Colored with Curcumin

The inorganic polymerization by sol–gel process involves molecular precursors (e.g., alkoxysilanes, in our case) which, through hydrolysis and polycondensation, generate an inorganic network and form a stable suspension of colloidal particles in a liquid phase. TEOS is the network generator, the component that hydrolyzes the fastest in acid catalysis and begins the formation of the silica network by homo-condensation or hetero-condensation with network modifiers (alkoxysilanes with one or two organic residues). Acid catalysis establishes a higher reaction rate for hydrolysis in relation to condensation, a process which leads to film-forming materials. Cyclic oligomerization of trialkoxysilanes leads to the formation of cyclic cages, while homo-polymerization of dialkoxysilanes leads

to linear highly flexible polymers that interpenetrate the silica network. Depending on the ratios between the modifiers and TEOS, the properties of the network, in which the dye is accommodated, are fine tuned. Therefore, it is possible to obtain silica film decorated with organic residues on the surface or as definite regions inside the silica network. The diffusion process of the molecules and, implicitly, the degree of connectivity in the network, are influenced, at the same time affecting the rate of the hydrolysis reaction [41–44].

The nanocomposite solutions were obtained by the sol–gel process, in acid catalysis, at room temperature. These resulted after 3 h by mixing the TEOS network initiator (1.6 mL) with the PTES network modifying agent (0.8 mL) and GPTES/DMDMS/DMDPS alternatives (0.8 mL) in the presence of 0.1 N HCl (0.75 g), using a mixture of EtOH (2.3 mL) and curcumin (0.02–0.06 g) dissolved in THF (2 mL). Three types of nanocomposites were obtained, differentiated by the type and amount of the second silica network modifier, P1 (GPTES), P2 (DMDMS), P3 (DMDPS). A total of 0.02 g of curcumin was used for these nanocomposites, which represents the optimal dye loading to obtain uniform polyester coatings. In the case of P1 composition, N-methylimidazole catalyst (0.01 mL) was used to accelerate the homo-polymerization of the epoxy ring, while in the case of P4, the mixture was obtained without the second type of network modifier. All the obtained solutions were deposited on the polyester support.

2.3. The Method of Depositing Nanosols on the Polyester Support

Each yellow, clear solution previously obtained, was deposited on 2 g polyester fabric at a wet pick-up of 38 to 42% by the pad-drying process. The dyeing parameters of the PES fabric were established on a horizontal laboratory padding mangle Ernst Bentz (Ernst Bentz AG, Kanton Zurich, Dielsdorf, Switzerland), at a constant speed of 0.5 m/min and a pressure of 0.4 kg/cm^2. The polyester fabric was passed several times through the dyeing solution, then it was dried at room temperature for 2 h. All coated materials were subjected to heat treatment at 120 °C for 1 h in a thermofixation oven.

2.4. Methods for Characterizing Dyed Polyester Fibers

FTIR-ATR spectrum measurements of nanosol coated fabrics were performed with a JASCO FT-IR 6300 instrument (Jasco Int. Co. Ltd., Tokyo, Japan), equipped with a Specac ATR Golden Gate (Specac Ltd., Orpington, UK) with KRS5 lens, in the range 400–4000 cm^{-1} (32 accumulations at a resolution of 4 cm^{-1}).

The coated fabrics were mapped using a microscope produced by VICKERS-JOYCE LOEBL (M17 Microscope, York, UK) and equipped with an OPTIKA (Optika C-B3, Ponteranica, Italy) 3Mpx optical camera, and the images are processed with ProView software (5.0, 2020, Opticaproview, Ponteranica, Italy).

Total color differences in CIELAB system, using a 10° standard observer and illuminant D65, transmittance and diffuse reflectance spectra, were measured with a V570 UV-VIS-NIR (Jasco Int. Co. Ltd., Tokyo, Japan) spectrophotometer equipped with a JASCO ILN-472 (150 mm) integrating sphere, using spectralon as reference and a fluorescence cut-off filter (U-330).

The fluorescence steady state properties of the covered fabrics were analyzed by recording fluorescence spectra on a JASCO FP 6500 spectrofluorimeter (Jasco Int. Co. Ltd., Tokyo, Japan), at 25 °C.

SEM images of coated polyester samples were obtained with a scanning electron microscope FEI QUANTA 200 (FEI, Hillsboro, OR, USA) at an accelerating voltage of 10–20 kV and at magnifications up to 10,000×.

The surface morphology of coated polyester was determined using a MultiMode 8 atomic force microscope (AFM) (Bruker, Santa Barbara, CA, USA). Measurements were carried out in Peak Force (PF) Quantitative Nanomechanical Mapping (QNM) mode, in air, at room temperature using silicon nitride tips at a scan rate of 1 Hz and a scan angle of 90°. The data and images were processed with NanoScope software (version 1.20, 2009, NanoScope Tech., Bedford, MA, USA).

Water contact angles (WCA) of films were determined with a CAM 200 (KSV Instruments, Helsinki Finland) equipped with a high resolution camera (Basler A602f, Basler, Ahrensburg, Germany) and an autodispenser. WCA was measured in air, at room temperature and ambient humidity, 2 s after the drop contacted the surface of the coatings. Drops of 6 µL deionized water were dispensed on each sample, and the value of the reported WCA was the average of six measurements.

Thermogravimetric analysis was performed with a TGA Q5000IR (TA Instruments, New Castle, DE, USA) instrument. The 3–5 mg samples were analyzed in platinum pans under the following conditions: ramp 10 °C/min to 700 °C, synthetic air 5.0 (99.999%) used as purge gas at a flow rate of 50 mL/min.

Dynamic mechanical analysis was performed on a TA Q 800 instrument (TA Instruments, New Castle, DE, USA), in DMA controlled force mode, by stress/strain method using a ramp force 1 N/min to 18 N and in multifrequencies strain mode using a film tension clamp, operated at a fixed frequency of 1 Hz, oscillation amplitude of 5 µm, temperature ramp of 30 °C/min., in air, from room temperature to 200 °C, on specimens of 10 mm × 10 mm × 50 mm.

Coated fabrics were evaluated for color fastness to washing and rubbing using ISO 105-C06 [45] and ISO-105X12 [46], respectively.

The four types of coated polyester fabrics were tested in accordance with the standards for determining the change in color after 4 cycles of repeated washing tests. The sample consisting of a piece of colored polyester fabric was placed between a piece of cotton and one of wool, each of it sewn on the four sides and the sandwich type sample was washed with an aqueous solution of 1% by weight sodium dodecylsulfate at 60 °C for 2 h, on a Linitest laboratory machine (Atlas, Rock Hill, IL, USA). After washing, the sample was rinsed with hot and cold water and allowed to air dry after unsewing it on three sides so that the fabric did not remain in contact with the accompanying materials. After drying, the samples were evaluated against the original colored fabrics.

The evaluation of the coated textiles for the protection degree against ultraviolet radiation was performed by measuring the transmittance spectra in the range of 280–400 nm and calculated according to the European standard for sun protective clothing: EN 13758-1.

3. Results and Discussion

In order to follow the adaptability process of film-forming materials containing the chromophore to the textile support, we synthesized four types of nanocomposites in which the silica network modifiers were varied. Curcumin was entrapped in the host silica matrices modified with aliphatic or aromatic residues. Following the process of impregnation with nanosol solutions, four types of uniformly coated polyester specimens were obtained (Figure 2a,b) having fluorescent properties (Figure 2c). The influence of the coatings' properties and interactions with the polyester support, related to the structure of nanocomposites, were also studied.

3.1. Structural Characterization of Coated Fabrics by FTIR Measurements

The four types of nanocomposite coated polyester materials were characterized by FTIR-ATR spectra to highlight the structural changes that occurred after the nanosol deposition onto the surface of the support (Figure 3).

The most intense signals were recorded at 1710 cm^{-1}, corresponding to the stretching vibration of the carbonyl group belonging to the ester bonds. At 1408, 1240, 1094 and 1016 cm^{-1} are identified absorption bands corresponding to bending vibration δ (C–O) and asymmetric stretching vibration ν_{as} (C–O–C). Bands of the valence vibrations characteristic to the C–H and C–C bonds of the aromatic rings are recorded at 872 and 720 cm^{-1}. The bands at 2962, 2915 and 2855 cm^{-1} correspond to the asymmetrical and symmetrical stretching vibrations of methylene groups. In addition, the small bands at 1504, 970 and 847 corresponds to C=C vibrational bands of the aromatic ring.

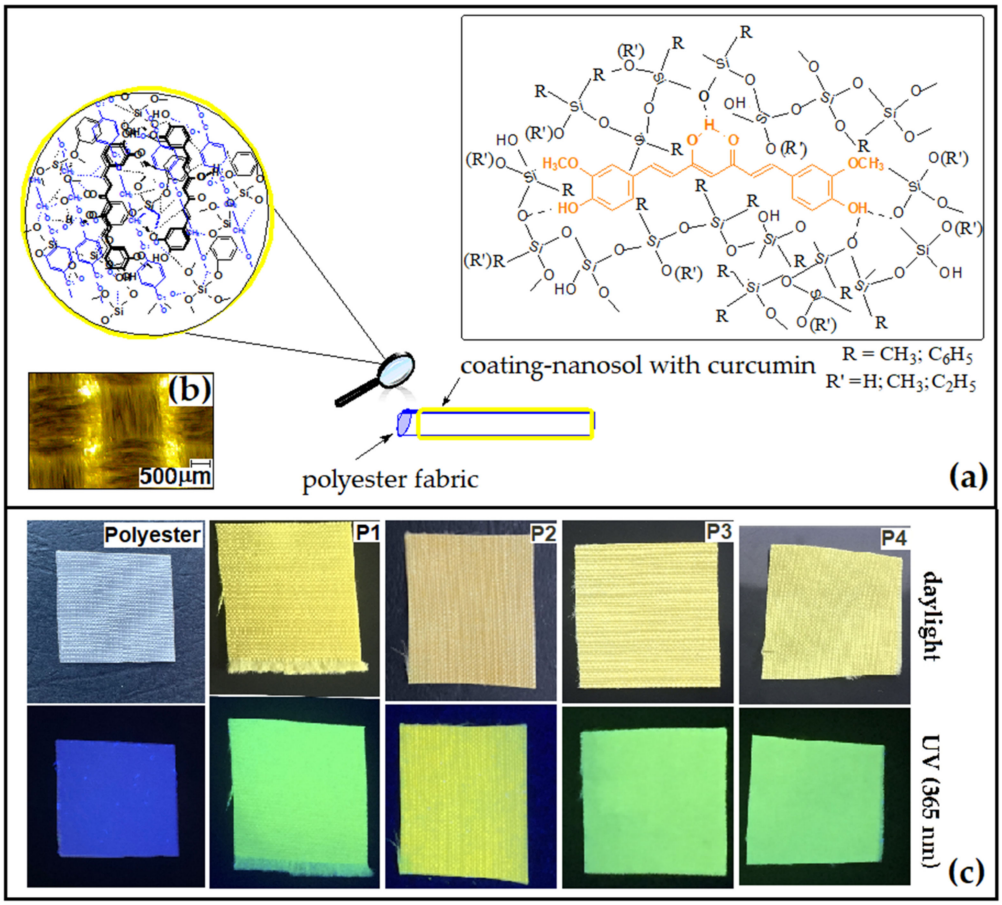

Figure 2. Nanocomposite coated polyester materials (**a**), optical image (**b**) and fluorescence emission during excitation at 365 nm (**c**).

All the signals presented are characteristic to polyester structures [7]. They have a different allure or intensity due to the interactions established with the signals given by the functional groups present in the composition of the nanosols. For this reason, the presence of Si–O–Si or Si–O–C groups, which have characteristic peaks at 1010–1020 cm^{-1}, 1120 cm^{-1}, respectively, cannot be highlighted. However, the presence of silica composites is confirmed by the structural changes recorded in the fingerprint area of the spectra. Therefore, in the range 650–600 cm^{-1}, wide bands corresponding to out of plane γ (OH) bending is recorded, O–Si–O bending is distinguished at 463 cm^{-1} and asymmetric stretching vibration ν_{as} (Si–O) is located at 519 cm^{-1}, all of them being characteristic bands of silicates [47–49]. FTIR spectrum and functional group characteristics are presented in the Supplementary Materials.

3.2. Morphology by SEM Analysis

The surface morphologies of raw and coated PES textile fabrics are presented in Figure 4. From SEM images, it was found that raw PES textile materials had a smooth and uniform surface. The diameter of the fibers is situated at around 20 µm. After coating the fibers, there can be observed a uniform film-forming material deposited along the fibers. Some agglomerates are seen on the surface, but they are sporadic and no larger than a micron. The origin of these agglomerates is the leakage of the film-forming material on the surface of the fibers and formation of some agglomerates such as "stem nodes". Therefore, for the same reason, some fabrics showed variations in the diameter of the yarns covered with nanosols.

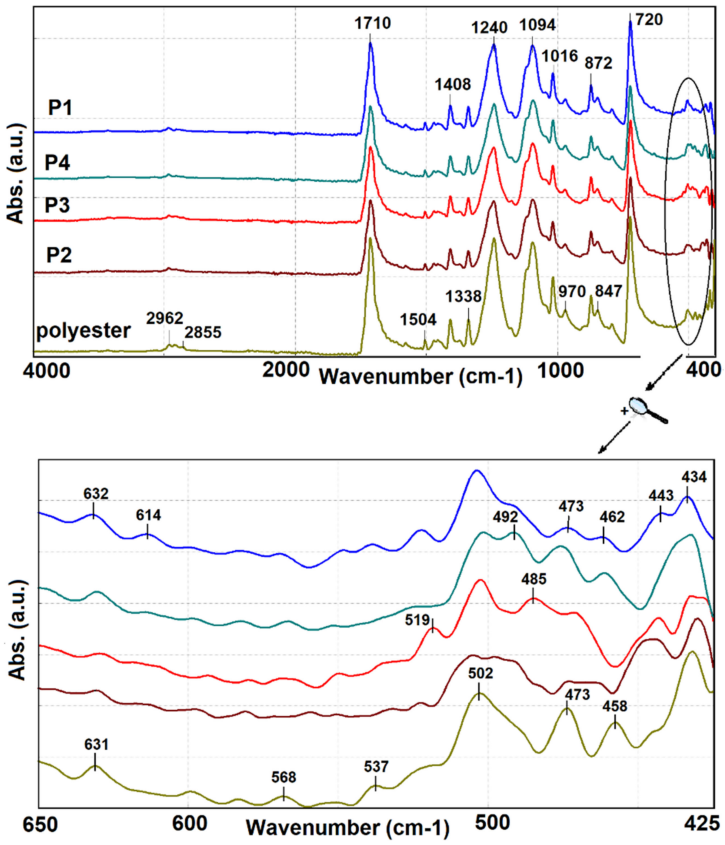

Figure 3. FTIR spectra for polyester fibers coated with nanosols.

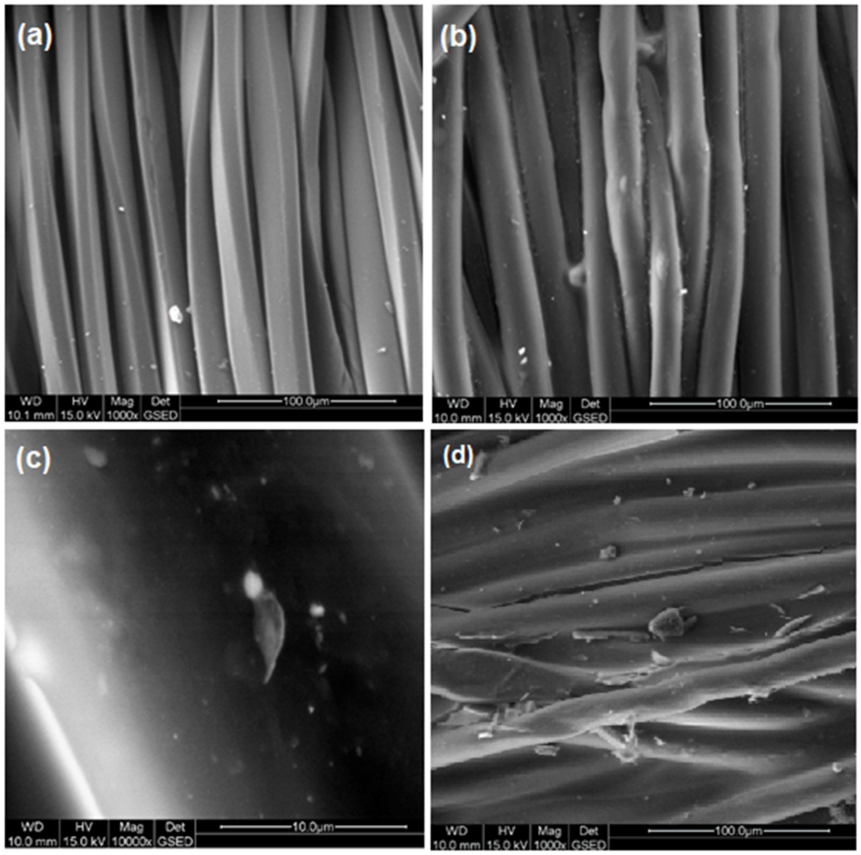

Figure 4. SEM micrographs of raw (**a**) and coated (**b**–**d**) PES textile fabrics.

The fluidity of the nanosol was necessary in order to be removed from the spaces between yarns by squeezing the impregnated fabric. Otherwise, it remains between wires with the formation of thick film-forming bridges, as it can be observed from Figure 4d. Such a situation leads to an increase in the rigidity of the fabric with a negative effect on the behavior of the fabric. The roughness of the film-forming material deposited onto the surface is determined by very small protrusions (tens of nanometers high), probably produced by the evaporation of solvents during crosslinking (as can be seen from the AFM images).

3.3. Morphological Properties of Nancoatings by AFM and Contact Angle Measurements

There are a lot of studies in literature regarding methods of treating polyester surfaces in order to increase the hydrophobicity of surfaces [9,50,51]. Of these, sol–gel coatings are well known and intensively studied and, therefore, in the present work, by varying the silica network modifiers, it is expected that coatings with hydrophobic properties will be obtained (Figure 5). Due to the morphology of the fabric, the polyester support used has hydrophilic properties and it was not possible to record the contact angle. Regarding the hydrophobic character, it was observed that the presence of GPTES in the nanosol composition during polymerization, in the presence of NMI, generated hydroxyl groups resulting from the opening of the epoxy ring, which determined the obtaining of more hydrophilic coatings than those with other organic groups.

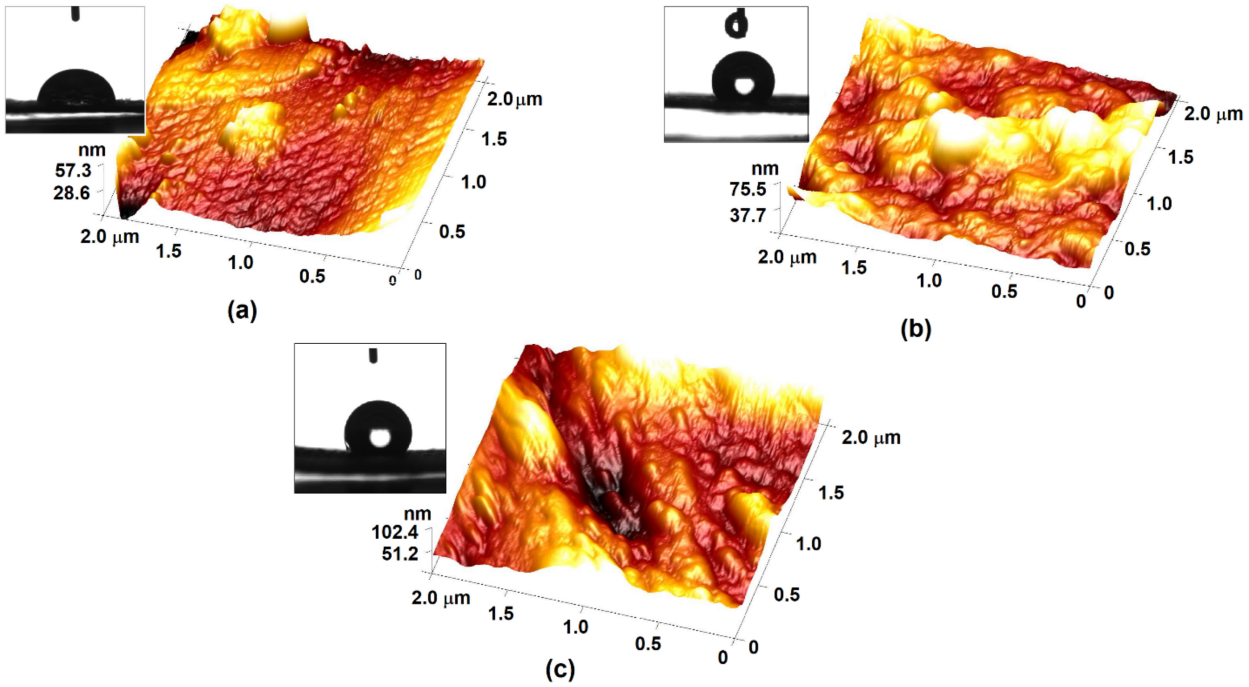

Figure 5. Topography AFM images and contact angle of water on P1 (**a**), P3 (**b**) and P4 (**c**).

The topographic analysis of the coatings highlights the formation of relatively thin films due to the linear structures of the polymeric chains generated in the presence of GPTES as a modifier of the silica network structure (Figure 5a).

It is observed that the presence of the voluminous groups introduced by PTES in the silica matrix led to π–π type stacking of the benzene rings, obtaining more thick coatings with a high peak around R_{max} = 102.4 nm (Figure 5c). At the same time, a reduction in the surface roughness of P4 compared to P1 is obtained, as it can be seen in Table 1. The interactions established between benzene rings from different molecules of precursors decisively determined a significant improvement in the hydrophobic properties of the coating, characterized by a WCA of 120° (Table 1). In the case of P2-type sol–gel coatings without dye (P2 blank), a very high value of 134 (±5.13°) of WCA was recorded (Figure 6).

This value does not change at high concentrations of the dye in the nanosol (135 ± 5.39°), but decreases significantly at low dye loadings (118 ± 8.1°). The change in the contact angle with the variation in the dye concentration can be explained by the hydrophobic nature of the dye, which leads to segregation processes in the silica matrix. At the same time, the structures of nanosols are also influenced by the processes of aggregation of dye molecules, at high loadings. While the concentration decreases, the dye is dispersed in the siloxane matrix and is willing to establish intermolecular bonds with the host matrix. By varying the ratio of alkyl and aryl residues in the siloxane matrix, it can be seen that the changes in the WCA of the coatings are not so dramatic, varying only by 5 to 7°.

Table 1. The square roughness and contact angle measured for the coated fabrics.

Compound	P1	P2	P3	P4
Square roughness (standard deviation), (nm)	79.75 (±1.1)	-	13.6 (±1.7)	21.37 (±6.2)
Contact angle (standard deviation), (°)	81 (±14.1)	118 (±8.1)	124 (±6.1)	120 (±14.8)

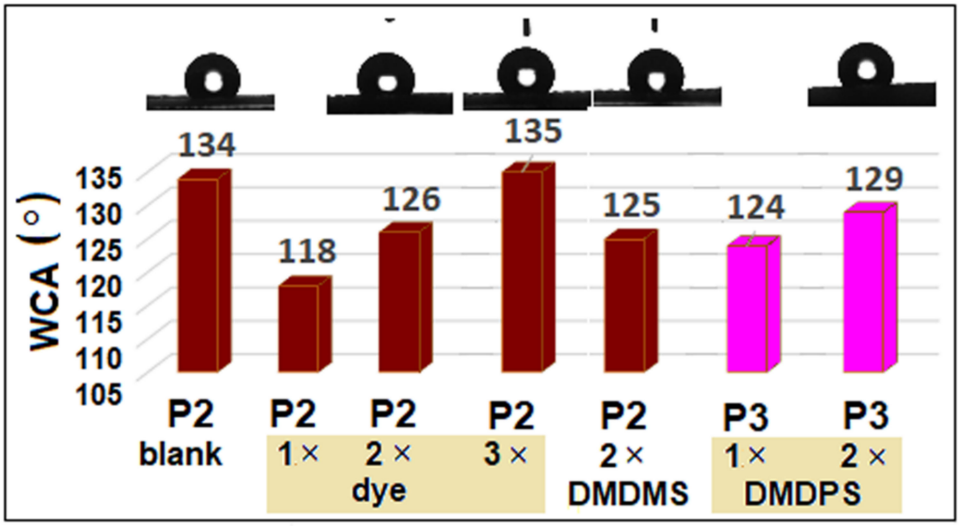

Figure 6. Modification of the hydrophobic properties of the coated polyester depending on the ratio between the components of the nanosol.

Increasing the ratio of benzene rings in the inorganic silica network, by adding 25% by weight DMDPS, leads to the generation of a more compact film, due to the generation of linear siloxane oligomers in an interpenetrated type structure. In this way, films with R_{max} = 75.5 nm, containing the aromatic groups probable to be oriented towards the film-air interface, are obtained. This arrangement determined, on the one hand, a more hydrophobic surface at the interface with air, and, on the other hand, a good compatibility with the PES support due to the π–π interactions with aromatic rings belonging to the polyester structure at the film–support interface. The P3 film has a lower roughness than P4, around 13.6 ± 1.7 nm, probably due to the compact arrangements of the organic groups and linear oligomers generated from the bifunctional network modifier DMDPS. These processes directly influenced the hydrophobic properties of the coated polyester fabric [7] and increased the WCA to about 124°.

3.4. Thermal Properties of Functionalized Polyester

3.4.1. Thermogravimetric Analysis of Composite Materials

The weight loss recorded during the thermal decomposition of polyester fibers comprises three stages and is somehow similar to that of nanosol (Figure 7). In the first step, up to 200 °C, mass loss is less than 1% and is attributed to water and residual solvents, following the thermal treatment of polyester fibers coated with nanosols. The second stage

is the main decomposition step and corresponds to a weight loss of about 80%. Due to curcuminoid hybrid systems, the last phase of decomposition for all four types of samples occurs at 5–10 °C later than in the case of uncovered PES. The amount of silica deposited on the fibers' surface can be estimated from the residue recorded at 700 °C and was situated at around 4% by weight.

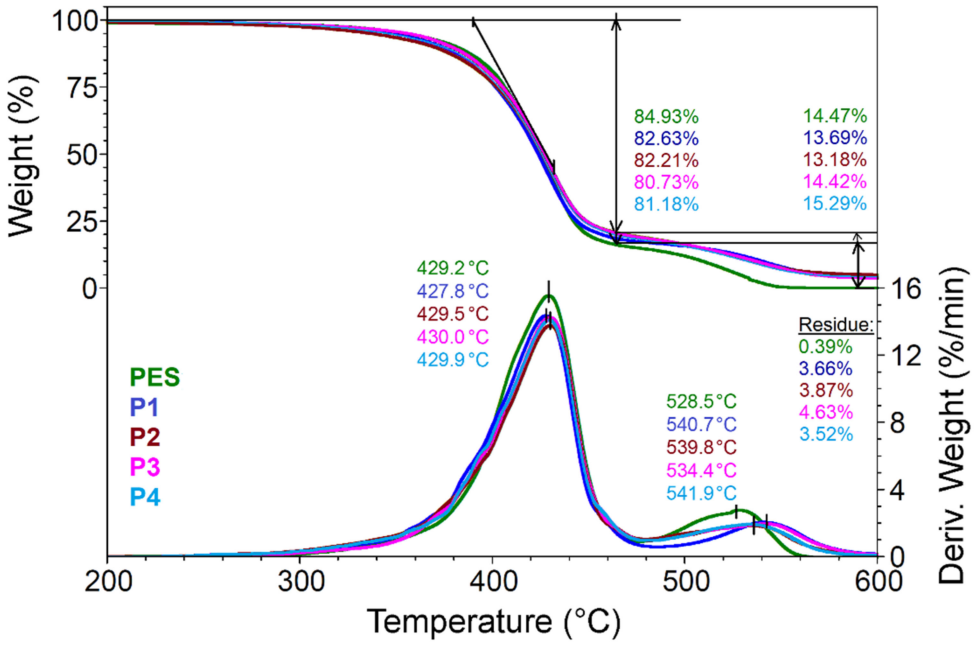

Figure 7. Thermogravimetric curves of hybrid materials.

Thus, it can be observed that the proportion of nanosol, in relation to the mass of the support on which it is deposited and its composition, does not significantly influence the thermal properties of the polyester fabric.

3.4.2. Thermomechanical Behavior of Coated Fabrics

The storage modulus is an indication referring to the ability of the samples to store deformation energy in an elastic manner and is closely related to the degree of crosslinking. In our study, at room temperature, the highest value of the storage modulus was recorded for P1 due to the formation of hydrogen bonds between hydroxyl groups generated by the homo-polymerization of epoxy groups and carbonyl groups belonging to the PES support. From the higher values obtained in the case of P3 or P2 compared to those obtained in the case of P4 (Figure 8a), it can be noticed that a higher degree of crosslinking of the hybrid coatings generated from trialkoxysilanes enhanced the storage modulus, while dialkoxysilane precursors, which generate linear siloxanes, lead to a more flexible coating. However, the π–π interactions, with the support, increased the storage relative to the support itself.

If we analyze the behavior of the storage modulus with temperature, we will notice that it is maintained within normal limits, without significant variations up to 110 °C, after which, due to exceeding the glass transition temperature of polyester fibers, there is a significant decrease in its value. In the particular case of P4, this phenomenon occurs later and variations are smaller.

The loss modulus (Table 2) is the dissipation component and its high values indicate that the sample is less stiff and the force is dissipated as heat. This is the case for the PES support, which has the highest value of loss modulus, while the next value is for P1, probably due to the large volume of homo-polymer generated from a glycidyl derivative, which leads to an increase in the free volume of the silica network stabilized by hydrogen bonds and to the possibility of dissipating energy through these bonds. In this case, the

loss modulus becomes higher because the energy lost through viscous heating is more important during the stressing process.

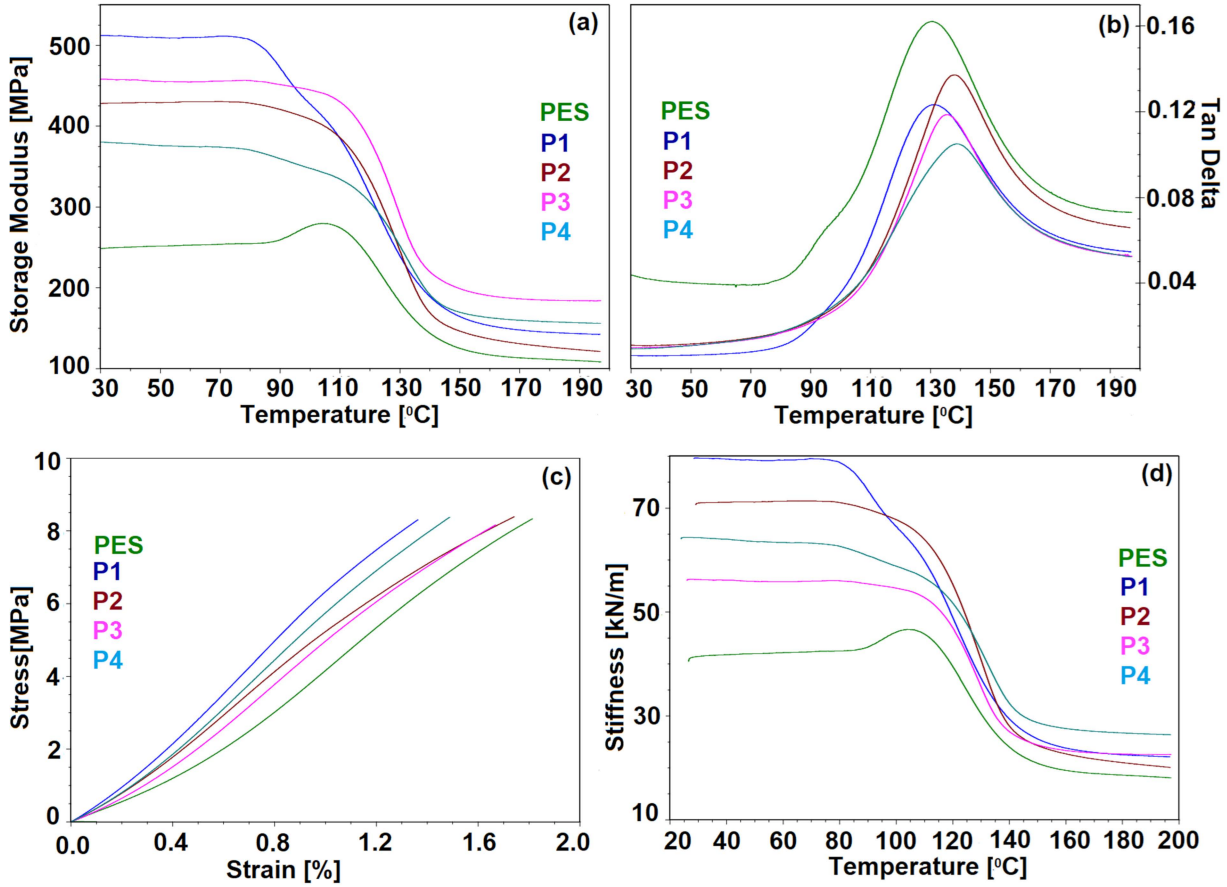

Figure 8. The thermomechanical properties of coated polyester fabrics, subjected to deformation forces (**a**,**b**), stress (**c**,**d**) vs. temperature.

Table 2. Storage modulus at 30 °C, 110 °C and 190 °C, loss modulus, tan delta and Young's modulus.

Sample	Storage Modulus (E′), MPa			Loss Modulus (E″)		Tan Delta		Young's Modulus
	30 °C	110 °C	190 °C	E″ (Peak Max), MPa	Temp, °C	Value	°C	GPa
PES	248.4	274.1	109.9	33.2	121.6	0.1622	131.0	0.5
P1	512.2	384.1	143.2	32.3	122.6	0.1234	131.3	0.66
P2	380.3	334.2	156.7	23.8	128.0	0.1051	138.7	0.51
P3	428	385.3	123.4	29.2	127.8	0.1373	138.0	0.53
P4	458.3	429.7	184.2	31.7	128.2	0.1187	135.5	0.61

As the peak height of the loss factor is associated with mobility, it was observed that, after the application of hybrid coatings, the molecular mobility was reduced, decreasing the possibility of energy dissipation through fiber–network interactions or by friction between fibers and, thus, the tan δ intensity decreases (Figure 8b). As stronger interactions are established between the coating and the polyester fabric, the peak is shifted to higher temperatures, with a direct consequence of improving the adhesion of the coating material to the textile substrate. It is obvious that the strongest interactions are established when using phenyl derivatives as modifying agents for the silica network.

However, the broader peaks recorded in all cases suggest molecular relaxations in the composites. From the stress–strain diagram (Figure 8c), it can be observed that the profile of the curves is almost linear and can be approximated by linear regression equations which

fit well experimental data, with R-squared values of more than 99%. From the slope of the curves Young's modulus was calculated (Table 2), which showed a softening of the hybrid coatings (P2, P3) when linear polymers are formed from DMDMS or DMDPS during the sol–gel process, while in the case of P1 a stiffening of the hybrid coating is recorded as a result of hydrogen bonds, as has already been established.

Overall, the intermolecular bonds between the coating material and the textile substrate occur predominantly through π–π type interactions, along with hydrogen bonds between the ester groups of the substrate and the silanol or hydroxyl groups generated during polymerization. This finding is of great importance from the perspective of obtaining coatings resistant to wet or dry detaching processes, as will be shown later.

3.5. Photophysical Properties of Nanosol Coated Fabrics

The samples obtained after impregnation were characterized by fluorescence emission and reflectance spectra. In this sense, the CIE standard color parameters (L*, a*, b*) were measured, using D65 as a light source and a 10° observer, and the obtained data are presented in Table 3. The textile samples were covered with different nanosols, but with the same type of chromophore show small differences in brightness, with hyper- and bathochromic effects. Depending on the silane components, the shade of the coatings changes slightly. As a result, the P2 coating, which contains alkyl residues in the silica network, is characterized by a positive value of the a* coordinate, and, therefore, presents a redness shift compared to the other coatings, in which aromatic residues are predominantly found. This property is due to the content of alkyl residues in the silica network, which interacts less with the functional groups of the dye sequestered in the silica network. At the same time, coatings in which aromatic residues are predominantly found, are characterized by high positive values of the b* coordinate, presenting shades shifted to yellow. Increasing the concentration of the dye in the nanosol leads to a decrease in brightness (L*). The obtained coatings have more reddish shades and are characterized by very high positive values of the a* coordinate and moderate increases in b*. These changes are caused by the intermolecular bonds established between the dye molecules, on the one side, and those established with the host matrix, on the other side. The latter are influenced by the structure of the matrix, respectively, and by the proportion of alkyl and aryl residues in the silica network. The presence of alkyl residues in P2 nanosols leads to the establishment of intermolecular hydrogen bonds with the dye and, thereby, a bathochromic shift is obtained. Moreover, due to the presence of the aryl residues in the silica network, the intermolecular bonds established with the dye are of the π–π type. Such nanosols lead to P3 type coatings with brighter shades, but with the hypsochromic shift in the color.

Table 3. Optical parameters of coated PES fabrics.

Sample	Color Parameters					Absorbance (λ_{max} 425 nm)	Fluorescence Emission (λ, nm)/(Intensity, a.u.)	Stokes Shif (SS, nm)	K/S
	L*	a*	b*	C*	h*				(a.u.)
PES	86.50	0.07	–2.57	2.57	271.45	-	-	-	-
P1	82.06	–9.58	38.89	40.05	103.84	0.4954	505 (921)	80	1.4878
P2	77.63	3.47	30.50	30.70	83.51	0.6713	515 (634)	90	1.6321
$P2_{(2\times Dye)}$	74.16	7.86	44.29	44.98	79.94	0.8336	530 (520)	105	-
$P2_{(3\times Dye)}$	72.68	11.52	45.82	47.24	75.88	0.8761	530 (442)	105	-
$P2_{(2\times DMDMS)}$	78.24	1.78	40.05	40.09	87.46	0.7123	515 (632)	90	-
P3	77.39	–5.01	36.82	37.16	97.74	0.6075	520 (542)	95	0.7310
$P3_{(2\times DMDPS)}$	74.87	4.92	34.60	34.95	81.92	0.7070	540 (651)	115	-
P4	81.94	–7.50	22.56	23.77	108.39	0.6941	550 (455)	125	1.1071

The coating P1, which was generated in the presence of GPTES, contains OH groups after the polymerization of epoxy rings and modifies the polarity of the host matrix, with

which the chromophore more easily established hydrogen bonds. These intermolecular interactions lead to a significant decrease in absorbance (Table 3).

The influence of the host matrix in which the dye is embedded on the optical properties of the coated fabrics were evaluated using Kubelka Munk equation (Figure 9). Considering that the dye concentration is constant and the textile support on which the hybrid materials were deposited was the same, it is observed that the light absorption and scattering processes are influenced by the structure of the siloxane network and, as a consequence, by the intermolecular interactions established between the dye, as a visiting molecule, and the hosting network. Thus, the predominant intermolecular hydrogen bonds in P1 lead to a decrease in the K/S value, compared to P2, where the organic network modifiers have lower potential to establish intermolecular hydrogen bonds with the chromophore. At the same time, the presence of phenyl groups in the siloxane network directly influenced the absorption coefficient of the dye. Their presence leads to a hydrophobic environment in the network that favors the aggregation processes due to π–π interactions between phenyl residues belonging to the dye and to the hybrid network. In this case, it can be observed that there is an increase in the ratio of phenyl groups in the P3 coating, which results in a drastic decrease in the K/S coefficient, compared to the P4 nanocomposite.

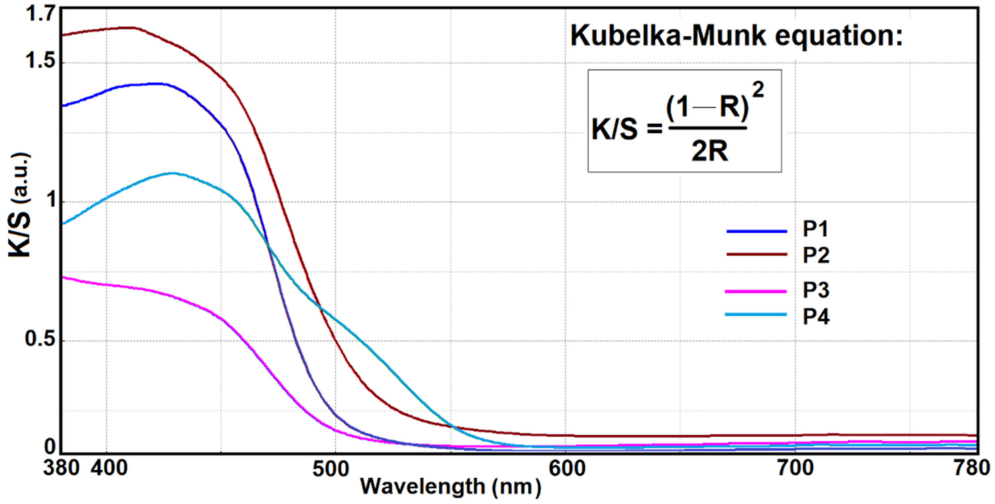

Figure 9. Color strength (K/S) of polyester textiles coated with hybrid materials and the Kubelka Munk equation, where K—absorption coefficient and S—scattering coefficient of the coated materials.

All the hybrid materials obtained by using the sol–gel process show fluorescence emissions (Figure 2c). The samples were measured at the same excitation wavelength, 435 nm, and the highest intensity was recorded at an emission wavelength of 505 nm for P1 (Table 3). Of the four types of nanosols, P4 has the highest Stokes shift (Δ ~ 125 nm) and the strongest bathofluoric shift. P1 and P2 hybrid materials, due to the presence of Si-OH and C–OH groups, the last one generated from epoxy homo polymerization and phenyl groups from PTES, create neighborhoods which interact with the fluorophore. Therefore, the type of interactions influences the fluorescence intensity of the chromophore (the influence of the solvent polarity or of the dye concentration are presented in the Supplementary Materials). It can be seen that, in the case of P3, coated with nanosol containing PTES and DMDPS network modifiers, the Stokes shift is not significantly modified compared to P4, containing only PTES shows a hypo- and bathofluoric shift in the emission maximum due to a limited interaction between the aromatic rings of the host matrix and the chromophore, which leads to a pathway of extinguishing fluorescence emission. However, it is observed that the increase in the alkyl residue ratio in the silica network does not influence the fluorescence intensity, 515 nm (632), while an excess of aryl residues in the siloxane matrix leads to a bathochromic effect (540 nm) and decreases the intensity of fluorescence emission. These results are due to the extensive intermolecular π–π type interactions.

Similar to the behavior of curcumin in polar solvents (shown in the Supplementary Materials), fluorescent properties were exhibited in siloxane matrices. The variation in the fluorescence emission intensity is determined by the polarity of the cavities in which curcumin is sequestered, but also by the concentration of the dye in the composition of the nanosol. The proximity of the dye in the hybrid matrix determines interactions and, thus, pathways to extinguish fluorescence [44].

The agglomeration of the cavities with voluminous substituents can cause the fluorescence of curcumin to be extinguished, even at low loadings. Increasing the volume of the cavities can lead to the possibility of extinguishing fluorescence through interactions between several dye molecules. The existence of the possibilities of interaction through hydrogen bonds between the dye molecules and Si–OH groups in the silica network also leads to a decrease in the fluorescence intensity (the main criterion according to which the optimal concentration of dye in the network was established). By choosing the optimal conditions for the formation of the network of film-forming material, the dye concentration can be adjusted to maximize fluorescence. Increasing the concentration of the dye in the siloxane matrix induces a bathochromic effect and leads to a decrease in fluorescence intensity (530 nm (442)). These fluorescence quenching processes are due to the dye aggregation phenomena that lead to segregation processes and the obtaining of uneven coatings. The same situation was encountered in the case of WCA measurements, where the most pronounced hydrophobic character was recorded at high dyestuff loadings, when aggregation became important. For this reason, the proportion of 0.02 g curcumin was chosen as the optimal amount used in nanosols of this type, to obtain uniform coatings with good optical properties.

3.6. Evaluation of Tinctorial Performances

By coating the polyester fibers with nanocomposites in the sol–gel system, intense and uniform colored materials were obtained. The four types of specimens were subjected to a process of four successive washing cycles, to evaluate the degree of leaching. After each washing cycle, the reflectance spectrum in the visible range was measured and the color strength (K/S) was evaluated (Figure 10). In this regard, it was found that the highest loss was suffered by the nanocomposite with DMDMS around 52%, while the other coatings containing aromatic rings in the structure of the silica network lost between 20%–30%. The best results were found in the case of the PTES modified film-forming material (loss of 22%). The stability of the film-forming material on the fibers was also verified by using the second method, which consists of measuring the color differences between the sample before and after performing the washing cycle. By comparing the total color differences, ΔE^*, it appears that they do not vary significantly in the case of P4 (Figure 10b), thus confirming that this nanocomposite has the best adhesion on polyester fibers. A superior performance was also observed after the friction tests. However, the sol–gel compositions with less voluminous alkyl groups had slightly better results both in dry and wet rubbing conditions (Table 4).

Table 4. Evaluation of coating resistance.

Sample	Washing Fastness (Grade) ISO 105 C06			Rubbing Fastness (Grade) ISO 105 X12	
	Color Change	Color Staining			
		Cotton	Wool	Dry	Wet
P1	4–5	4–5	4–5	4–5	4
P2	4	4	4–5	4–5	4–5
P3	4–5	4–5	4–5	4	3
P4	4	4	4–5	3–4	3

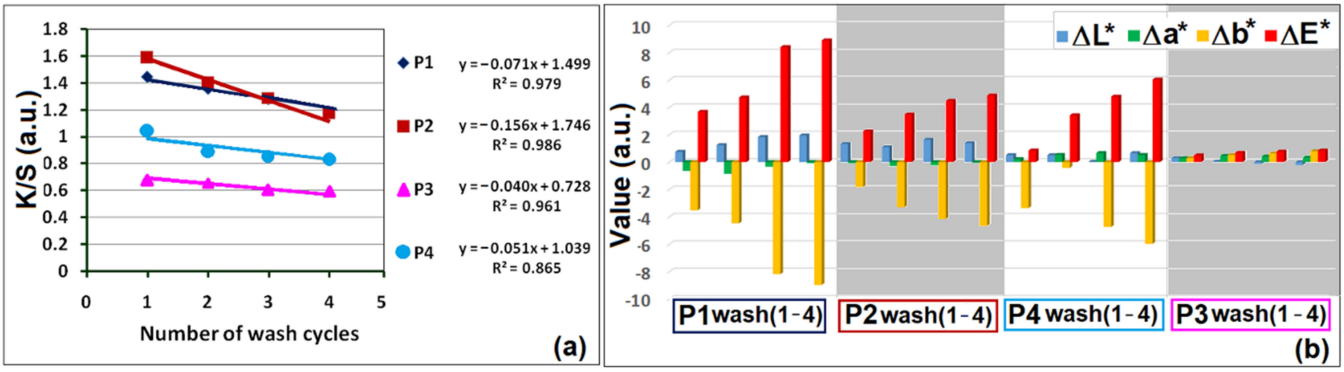

Figure 10. Evaluation of the films' resistance during repeated washing cycles by the measurement of K/S values (**a**) and ΔE* in CIEL*a*b* system (**b**).

The very good results obtained after repeated washing and abrasion tests show that film-forming materials have good adhesion on polyester fibers. These properties are due to the intermolecular interactions established between the silica network and the skeletal or functional groups of the polyester fibers. From the results, it can be seen that nanosols containing linear polymers or functional groups that cannot hinder intermolecular interactions between coatings and support, generate film-forming materials with improved adhesion properties.

3.7. Sun Protective Performances Evaluation

In the early 2000s, the awareness of the need for protection against ultraviolet radiation became more than evident. This was due to the increase in the number of skin cancer cases and other dermatological conditions following sun exposure [52–54]. Regarding this process, the level of protection was studied depending on the fabric and the type of coatings. Thus, it has been observed that polyester fabrics had a higher protection factor than cotton [55]. At the same time, different types of coatings were made using modern methods, using absorbers or blockers to improve the anti-UV properties [56–60].

The ultraviolet protection factor (UPF) for each polyester specimen (Figure 11) was calculated based on the measured transmittance spectra. The protection level of the covered textiles was calculated (Figure 12), according to the European Standard EN 13758-1.

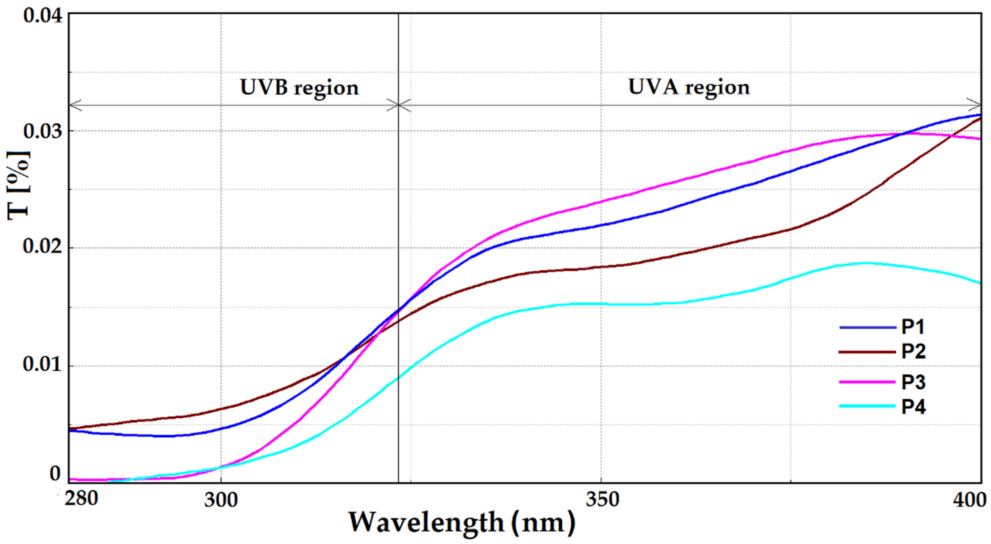

Figure 11. The transmittance spectra of coated fabrics.

$$UPF = \frac{\sum_{\lambda = 290}^{\lambda = 400} E(\lambda(\lambda)\varepsilon(\lambda))}{\sum_{\lambda = 290}^{\lambda = 400} E(\lambda(\lambda)T(\lambda)\lambda)\Delta\lambda}$$

Figure 12. Equation for the calculation of the ultraviolet protection factor (UPF), where $E(\lambda)$ is the solar spectral irradiance; $\varepsilon(\lambda)$ is the relative erythema effectiveness; $T(\lambda)$ is the spectral transmittance at wavelength; and $\Delta\lambda$ is the wavelength interval of the measurements.

From the shape of the transmittance spectra, it can be intuited that the coatings have anti-UV properties. This subheading (forecast) is supported by the very low transmittance T < 0.02% in the UVB range (290–320 nm), whose values in the UVA region (Figure 11) reach around 0.03%. Thus, following the calculations in which the values of the transmitters in the range 290–400 nm are involved, according to EN 13758-1, these results confirm that all the coated polyester textiles have the ultraviolet protection factor +50 (Figure 13).

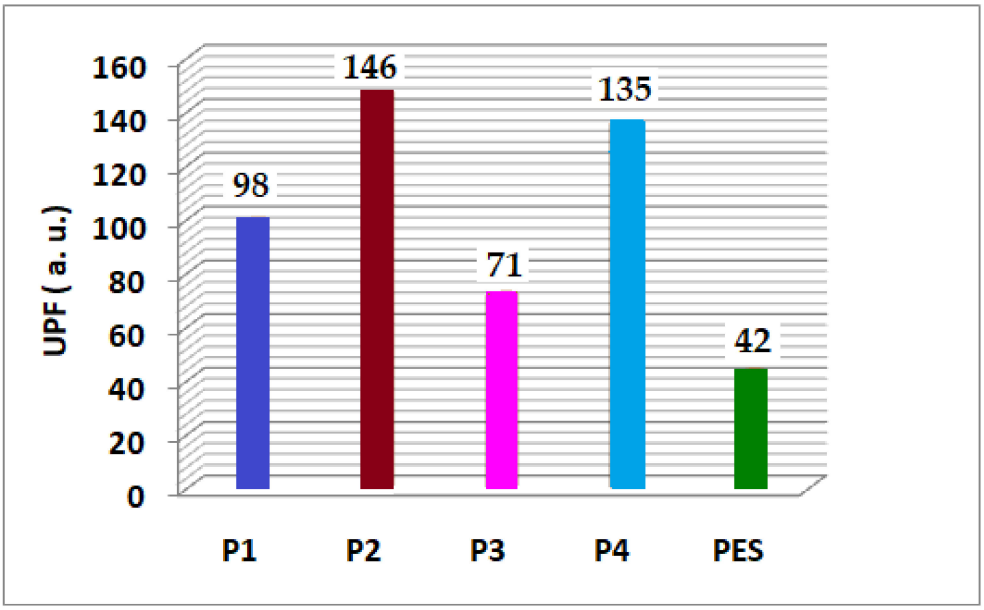

Figure 13. UV protection factor of coated textiles calculated according to EN 13758-1.

As can be found in literature [60], the sol–gel type coatings do not have anti-UV properties, but are used for this purpose by modifying the silica network with different inorganic anti-UV blockers, in the form of nanoparticles or organic absorbents of preferred dyes with antioxidant properties. In this case, the curcumin chromophore shows absorption in the ultraviolet region and has embedded in the siloxane matrix, conferring very good protection properties against ultraviolet radiation. Another factor that leads to the protective performances is probably the loading of the gaps between the fabric threads following the process of the deposition of nanocomposites on the polyester support (showed earlier in Figure 2b). In evaluating the anti-UV protection factor that fabrics offer, the effect over time is very important. It is closely related to the washing resistance of film-forming materials on the support. Considering the very good resistance properties after the washing process, measurements of the transmittance for P3 were performed and, following the calculations, it was confirmed that, after four repeated washing cycles, the coated polyester specimen maintain an UPF +50.

4. Conclusions

The fluorescent properties of the chromophore were preserved even after the process of embedding in the siloxane matrix. It was demonstrated that the optical properties of the coatings can be fine tuned by varying the type and the amount of silica network modifiers.

The thermomechanical properties of the coated fabrics can be varied because they are heavily influenced by the composition of the film-forming materials and, consequently, by the interactions established between coatings and textile support.

Polyester fabrics coated with hybrid curcuminoid systems have a hydrophobic surface, have fluorescent properties and an UPF +50, so they can be used in various fields where it is necessary for textiles to have signaling, self cleaning or protection against ultraviolet radiation.

The polyester fabrics on which the hybrid materials were deposited have very good properties, in terms of the resistance to repeated washing cycles, and maintain the original UV protection factor at high values even after four washing cycles, or during rubbing tests.

Supplementary Materials: The following supporting information can be downloaded at: https://www.mdpi.com/article/10.3390/coatings12020271/s1, Scheme S1: Chemical structure of a hybrid film forming material (P3 blank); Figure S1: FTIR-ATR spectrum of curcumin; Figure S2: Thermal stability of PES fibers and P1 before and after thermal treatment at 120 °C by DSC measurements: (a) 1st heating cycle, (b) 1st cooling cycle, (c) 2nd heating cycle; Figure S3: TGA analysis of P3 hybrid material; Figure S4: Intensity of curcumin fluorescence emission and peak maximum wavelength in solvents with different polarities (a), influence of curcumin concentration on fluorescence emission (b). Reference [61] is cited in the Supplementary Materials.

Author Contributions: Conceptualization, F.M.R. and V.R.; methodology, A.R. and V.P.; validation, V.R., A.R. and V.P.; formal analysis, G.I., A.N.F., C.-A.N., R.A.G.; investigation, F.M.R., A.N.F., V.P.; writing—original draft preparation, F.M.R. and A.R.; writing—review and editing, V.R. and V.P.; supervision, V.R.; project administration, F.M.R., A.R. All authors have read and agreed to the published version of the manuscript.

Funding: This work was supported by a grant of the Ministry of Research, Innovation and Digitization, CNCS/CCCDI—UEFISCDI, project number PN-III-P2-2.1-PED-2019-1471, within PNCDI III and by the INCDCP ICECHIM Bucharest 2019-2022 Core Program PN. 19.23–Chem-Ergent, Project No.19.23.03.04.

Institutional Review Board Statement: Not applicable.

Informed Consent Statement: Not applicable.

Data Availability Statement: Data sharing is not applicable to this article.

Conflicts of Interest: The authors declare no conflict of interest.

References

1. Rashid, M.A.; Hossain, D.; Islam, M.M.; Hasan, N.U. Evaluation of economical and ecological aspects of denim garments dyeing with fluorescent dye. *J. Mater. Sci. Eng.* **2013**, *1*, 1–6. [CrossRef]
2. Hamdaoui, M.; Lanouar, A.; Halaoua, S. Study of fluorescent dyeing process and influence of mixture dyes on high-visibility. *J. Eng. Fibers Fabr.* **2015**, *10*, 89–96. [CrossRef]
3. Atta-Eyison, A.A. Performance evaluation of fluorescence and photostability of coumarin Disperse Yellow 82. *J. Mater. Sci. Eng.* **2020**, *8*, 11–19. [CrossRef]
4. Szuster, L.; Kaźmierska, M.; Król, I. Fluorescent dyes destined for dyeing high-visibility polyester textile products. *Fibres Text East. Eur.* **2004**, *12*, 1.
5. Shree, L.G.; Ashok, K.A.; Prithivraj, G.; Vipin, V.; Sathish, K.M. Fluorescent dyeing in polyester and cotton blended fabrics. *Int. Res. J. Eng. Technol.* **2020**, *7*, 5.
6. Aysha, T.; Zain, M.; Arief, M.; Youssef, Y. Synthesis and spectral properties of new fluorescent hydrazone disperse dyes and their dyeing application on polyester fabrics. *Heliyon* **2019**, *5*, e02358. [CrossRef]
7. Raditoiu, A.; Amariutei, V.; Raditoiu, V.; Ghiurea, M.; Frone, A.N.; Gabor, R.A.; Wagner, L.E.; Anastasescu, M. Polyester fibers coated with silica hybrid film forming materials containing non-ionic dyes. *J. Optoelectron. Adv. Mater.* **2015**, *17*, 198–204.
8. Boukhriss, A.; Boyer, D.; Hannache, H.; Roblin, J.P.; Mahiou, R.; Cherkaoui, O.; Therias, S.; Gmouh, S. Sol–gel based water repellent coatings for textiles. *Cellulose* **2015**, *22*, 1415–1425. [CrossRef]

9. Za'im, N.N.M.; Yusop, H.M.; Ismail, W.N.W. Synthesis of water-repellent coating for polyester fabric. *Emerg. Sci. J.* **2021**, *5*, 5. [CrossRef]
10. Nejman, A.; Kamińska, I.; Giesz, P.; Cieślak, M. Thermal stability of polyester fabric with polyacrylic coatings. *Fibres Text East. Eur.* **2015**, *23*, 73–82. [CrossRef]
11. Periyasamy, A.P.; Venkataraman, M.; Kremenakova, D.; Militky, J.; Zhou, Y. Progress in sol-gel technology for the coatings of fabrics. *Materials* **2020**, *13*, 1838. [CrossRef]
12. Kale, R.D.; Agnihotri, A.; Jagtap, P.S. Simultaneous dyeing and anti-bacterial finishing of textile by sol-gel technique. *Adv. Appl. Sci. Res.* **2016**, *7*, 116–122.
13. Salem, T.; El-Kashouty, M.; Müller, M.; Simon, F. Sol-gel synthetic route to improve interaction of polyester/cotton blended fabric with anionic dyes. *Egypt. J. Chem.* **2017**, *60*, 1151–1164. [CrossRef]
14. Patela, B.H.; Patela, P.N.; Chaudharib, S.B.; Mandot, A.A. Nano silica mediated sol-gel dyeing of cotton and polyester fabric. *Int. Dyer* **2016**, *3*, 38–41.
15. Raditoiu, A.; Raditoiu, V.; Amariutei, V.; Purcar, V.; Ghiurea, M.; Raduly, M.; Wagner, L. Surface coating on cellulose fabrics with nonionic dyes—Silica hybrids. *Mater. Plast.* **2015**, *52*, 442–448.
16. Santos, C.; Brum, L.F.W.; Vasconcelos, R.F.; Velho, S.K.; Santos, J.H.Z. Color and fastness of natural dyes encapsulated by a sol-gel process for dyeing natural and synthetic fibers. *J. Sol-Gel Sci. Technol.* **2018**, *86*, 351–364. [CrossRef]
17. Elnagar, K.; Elmaaty, T.A.; Raouf, S. Dyeing of polyester and polyamide synthetic fabrics with natural dyes using ecofriendly technique. *J. Text.* **2014**, *2014*, 8. [CrossRef]
18. Karthikeyan, G.; Vidya, A.K. Production and application of natural dye from skin of yellow pumpkin vegetable. *Int. J. Recent Sci. Res.* **2020**, *11*, 37828–37839.
19. Batool, F.; Iqba, N.; Azeem, M.; Adeel, S.; Ali, M. Sustainable dyeing of cotton fabric using Black Carrot (*Daucus carota* L.) plant residue as a source of natural colorant. *Pol. J. Environ. Stud.* **2019**, *28*, 3081–3087. [CrossRef]
20. Bhuiyan, M.A.R.; Ali, A.; Islam, A.; Hannan, M.A.; Kabir, F.S.M.; Islam, M.N. Coloration of polyester fber with natural dye henna (*Lawsonia inermis* L.) without using mordant: A new approach towards a cleaner production. *Fash Text.* **2018**, *5*, 2. [CrossRef]
21. Tambi, S.; Mangal, A.; Singh, N.; Sheikh, J. Cleaner production of dyed and functional polyester using natural dyes vis-avis exploration of secondary shades. *Prog. Color. Colorants Coat.* **2021**, *14*, 121–128.
22. Samanta, P.; Singhee, D.; Samanta, A.K. Fundamentals of natural dyeing of textiles: Pros and Cons. *Curr. Trends Fashion Technol. Textile Eng.* **2018**, *2*, 4. [CrossRef]
23. Hasan, M.; Hossain, M.B.; Azim, A.Y.M.A.; Ghosh, N.C.; Reza, S. Application of purified curcumin as natural dye on cotton and polyester. *Int. J. Eng. Technol.* **2014**, *14*, 5.
24. Alsamydai, A.; Jaber, N. Pharmacological aspects of curcumin: Review article. *Alsamydai Jaber* **2018**, *5*, 313–326. [CrossRef]
25. Rathore, S.; Mukim, M.; Sharma, P.; Devi, S.; Nagar, J.C.; Khalid, M. Curcumin: A review for health benefits. *Int. J. Inf. Res. Rev.* **2020**, *7*, 1.
26. Sharifi-Rad, J.; Rayess, Y.E.; Rizk, A.A.; Sadaka, C.; Zgheib, R.; Zam, W.; Sestito, S.; Rapposelli, S.; Neffe-Skocin´ska, K.; Zielin´ska, D.; et al. Turmeric and its major compound curcumin on health: Bioactive effects and safety profiles for food, pharmaceutical, biotechnological and medicinal applications. *Front. Pharmacol.* **2020**, *11*, 01021. [CrossRef] [PubMed]
27. Shibayama, N.; Wypyski, M.; Gagliardi-Mangilli, E. Analysis of natural dyes and metal threads used in 16th-18th century Persian/Safavid and Indian/Mughal velvets by HPLC-PDA and SEM-EDS to investigate the system to differentiate velvets of these two cultures. *Herit. Sci.* **2015**, *3*, 12. [CrossRef]
28. Raduly, F.M.; Raditoiu, V.; Raditoiu, A.; Purcar, V. Curcumin: Modern applications for a versatile additive. *Coatings* **2021**, *11*, 519. [CrossRef]
29. Gupta, A.; Briffa, S.M.; Swingler, S.; Gibson, H.; Kannappan, V.; Adamus, G.; Kowalczuk, M.M.; Martin, C.; Radecka, I. Synthesis of silver nanoparticles using curcumin-cyclodextrins loaded into bacterial cellulose-based hydrogels for wound dressing applications. *Biomacromolecules* **2020**, *21*, 1802–1811. [CrossRef]
30. El-Nahhal, I.M.; Salem, J.; Anbar, R.; Kodeh, F.S.; Elmanama, A. Preparation and antimicrobial activity of ZnO-NPs coated cotton/starch and their functionalized ZnO-Ag/cotton and Zn (II) curcumin/cotton materials. *Sci. Rep.* **2020**, *10*, 1–10. [CrossRef]
31. Ahmed, S.S.Z.; Balu, N.; Khader, S.Z.A.; Mahboob, M.R.; Lakshmanan, S.O.; Vetrivel, M. Fabrication and evaluation of bamboo fabric coated with extracts of Curcuma longa, Centella asiatica and Azadirachta indica as a wound dressing material. *Adv. Tradit. Med.* **2021**, *21*, 83–95. [CrossRef]
32. Li, S.; Lu, M.; Hu, R.; Tang, T.; Hou, K.; Liu, Y. Dyeing ramie fabrics with curcumin in NaOH/urea solution at low temperature. *Cloth. Text. Res. J.* **2019**, *37*, 66–79. [CrossRef]
33. Wang, M.; Liu, M.; Zhao, H.; Xiong, X.; Zheng, L. Reactive modified curcumin for high-fastness nonaqueous SC-CO2 dyeing of cotton fabric. *Cellulose* **2020**, *27*, 10541–10551. [CrossRef]
34. Gotmare, V.D.; Kole, S.S.; Athawale, R.B. Sustainable approach for development of antimicrobial textile material using nanoemulsion for wound care applications. *Fash Text.* **2018**, *5*, 25. [CrossRef]
35. Diaa, M.; Othman, H.A.; Hassabo, A.G. Printing wool fabrics with natural dyes curcuma and alkanet (A Critique). *J. Text. Color. Polym. Sci.* **2022**, *19*, 11–16. [CrossRef]
36. Galasso, V.; Kovac, B.; Modelli, A.; Ottaviani, M.F.; Pichierri, F. Spectroscopic and theoretical study of the electronic structure of curcumin and related fragment molecules. *J. Phys. Chem. A* **2008**, *112*, 2331–2338. [CrossRef]

37. Rege, S.A.; Arya, M.; Momin, S.A. Structure activity relationship of tautomers of curcumin: A review. *Ukr. Food J.* **2019**, *8*, 1. [CrossRef]
38. Michels, L.; Richter, A.; Chellappan, R.K.; Røst, H.I.; Behsen, A.; Wells, K.H.; Leal, L.; Santana, V.; Blawid, R.; da Silva, G.J.; et al. Electronic and structural properties of the natural dyes curcumin, bixin and indigo. *RSC Adv.* **2021**, *11*, 14169. [CrossRef]
39. Gál, E.; Nagy, L.C. Photophysical properties and electronic structure of symmetrical curcumin analogues and their BF2 complexes, including a phenothiazine substituted derivative. *Symmetry* **2021**, *13*, 2299. [CrossRef]
40. Raduly, M.F.; Raditoiu, V.; Raditoiu, A.; Wagner, L.E.; Amariutei, V.; Ailiesei Darvaru, G. Facile synthesis of curcumin and curcuminoid-like derivatives at microwaves. *Rev. Chim.* **2018**, *69*, 1327–1331. [CrossRef]
41. Baig, N.; Kammakakam, I.; Falath, W. Nanomaterials: A review of synthesis methods, properties, recent progress, and challenges. *Mater. Adv.* **2021**, *2*, 1821. [CrossRef]
42. Bokov, D.; Jalil, A.T.; Chupradit, S.; Suksatan, W.; Ansari, M.J.; Shewael, I.H.; Valiev, G.H.; Kianfar, E. Nanomaterial by Sol-Gel Method: Synthesis and Application. *Adv. Mater. Sci. Eng.* **2021**, *2021*, 5102014. [CrossRef]
43. Tan, W.K.; Muto, H.; Kawamura, G.; Lockman, Z.; Matsuda, A. Nanomaterial Fabrication through the Modification of Sol–Gel Derived Coatings. *Nanomaterials* **2021**, *11*, 181. [CrossRef]
44. Raduly, F.M.; Raditoiu, V.; Raditoiu, A.; Frone, A.N.; Nicolae, C.A.; Purcar, V.; Ispas, G.; Constantin, M.; Raut, I. Modeling the Properties of Curcumin Derivatives in Relation to the Architecture of the Siloxane Host Matrices. *Materials* **2022**, *15*, 267. [CrossRef] [PubMed]
45. *ISO 105-C06*; ISO Textiles—Test for Color Fastness—Part C06: Colour Fastness to Domestic and Commercial Laundering. International Organization for Standardization: Geneva, Switzerland, 2010.
46. *ISO 105-X12*; ISO Textiles—Tests for Colour Fastness—Part X12: Colour Fastness to Rubbing. International Organization for Standardization: Geneva, Switzerland, 2016.
47. Yin, Y.; Yin, H.; Wu, Z.; Qi, C.; Tian, H.; Zhang, W.; Hu, Z.; Feng, L. Characterization of coals and coal ashes with high Si content using combined second-derivative infrared spectroscopy and Raman spectroscopy. *Crystals* **2019**, *9*, 513. [CrossRef]
48. Hofmeister, A.M.; Bowey, J.E. Quantitative infrared spectra of hydrosilicates and related minerals. *Mon. Not. R. Astron. Soc.* **2006**, *367*, 577–591. [CrossRef]
49. Apopei, A.I.; Buzgar, N.; Buzatu, A. Raman and infrared spectroscopy of kaersutite and certain common amphiboles. *AUI Geol.* **2011**, *57*, 35–58.
50. Ma, Q.; Wang, B.; Xu, J.; Lv, J.; Li, H.; Li, Y.; Zhao, C. Preparation of super-hydrophobic polyester fabric by growing polysiloxane microtube and its application. *Silicon* **2018**, *10*, 2009–2014. [CrossRef]
51. Xu, L.; Xie, K.; Liu, Y.; Zhang, C. Stable super-hydrophobic and comfort PDMS-coated polyester fabric. *e-Polymers* **2021**, *21*, 654–661. [CrossRef]
52. Gies, P.; Roy, C.; McLennan, A.; Pailthorpe, M.; Hilfikery, R.; Osterwalderz, U.; Monard, B.; Moseley, H.; Sliney, D.; Wengraitis, S.; et al. Ultraviolet protection factors for clothing: An intercomparison of measurement systems. *Photochem. Photobiol.* **2003**, *77*, 58–67. [CrossRef]
53. Gambichler, T.; Rotterdam, S.; Altmeyer, P.; Hoffmann, K. Protection against ultraviolet radiation by commercial summer clothing: Need for standardised testing and labeling. *BMC Dermatol.* **2001**, *1*, 6. [CrossRef]
54. Gambichler, T.; Avermaete, A.; Bader, A.; Altmeyer, P.; Hoffmann, K. Ultraviolet protection by summer textiles. Ultraviolet transmission measurements verified by determination of the minimal erythema dose with solar-simulated radiation. *Br. J. Dermatol.* **2001**, *144*, 484–489. [CrossRef]
55. Davis, S.; Capjack, L.; Kerr, N.; Fedosejevs, R. Clothing as protection from ultraviolet radiation: Which fabric is most effective? *Int. J. Dermatol.* **1997**, *36*, 374–379. [CrossRef]
56. Sarkar, A.K. On the relationship between fabric processing and ultraviolet radiation transmission. *Photodermatol. Photoimmunol. Photomed.* **2007**, *23*, 191–196. [CrossRef]
57. Grifoni, D.; Bacci, L.; Zipoli, G.; Carreras, G.; Baronti, S.; Sabatini, F. Laboratory and outdoor assessment of UV protection offered by flax and hemp fabrics dyed with natural dyes. *Photochem. Photobiol.* **2009**, *85*, 313–320. [CrossRef]
58. Mavrić, Z.; Tomšič, B.; Simončič, B. Recent advances in the ultraviolet protection finishing of textiles. *Tekstilec* **2018**, *61*, 201–220. [CrossRef]
59. Olczyk, J.; Sójka-Ledakowicz, J.; Walawska, A.; Antecka, A.; Siwi´nska-Ciesielczyk, K.; Zdarta, J.; Jesionowski, T. Antimicrobial activity and barrier properties against UV radiation of alkaline and enzymatically treated linen woven fabrics coated with inorganic hybrid material. *Molecules* **2020**, *25*, 5701. [CrossRef]
60. Mahltig, B.; Leisegang, T.; Jakubik, M.; Haufe, H. Hybrid sol-gel materials for realization of radiation protective coatings—A review with emphasis on UV protective materials. *J. Sol-Gel Sci. Technol.* **2021**. [CrossRef]
61. Gunasekaran, S.; Natarajan, R.K.; Natarajan, S.; Rathikha, R. Structural Investigation on Curcumin. *Asian J. Chem.* **2008**, *20*, 2903–2913.